Climate Dynamics (2026) 64:367
https://doi.org/10.1007/s00382-026-08335-5

The unique effect of Atlantic forcing on Central Pacific El Niño

Qi Tian[1,2] · Jiawei Tang[1,2] · Ruiqiang Ding[1,2] · Jianping Li[3] · Liang Shi[4,5]

Received: 8 April 2026 / Accepted: 3 August 2026 / Published online: 11 August 2026

Abstract
Understanding the surge in Central Pacific (CP) El Niño events after the 1990s is a pivotal concern in climate science. However, the relationship between the Atlantic air-sea signals and the CP El Niño remains poorly explained systematically. Here, we show that the Atlantic air-sea signals exhibit a strong correlation with CP El Niño variability after the 1990s. During the initial preconditioning phase, the positive phase of the North Atlantic Oscillation (NAO) in the preceding winter drives the emergence of the spring negative North Tropical Atlantic (NTA) SST anomalies, which trigger the initial warming in the central Pacific. During the development phase, the persistent easterly anomalies in the equatorial eastern Pacific associated with the NTA SST anomalies disrupt the functioning of zonal advection feedback in the equatorial eastern Pacific. As a consequence, this contributes to the formation of a CP El Niño event. Therefore, the increased prevalence of CP El Niño events after the 1990s can be attributed to the unique role of easterly anomalies over the equatorial eastern Pacific, a key process influenced by Atlantic air-sea signals. This finding advances our understanding of CP El Niño dynamics and contributes to more precise climate predictions and meteorological risk assessments.

Keywords Central Pacific El Niño · Atlantic air-sea signals · North Atlantic oscillation · North Tropical Atlantic

1 Introduction

El Niño-Southern Oscillation (ENSO) events are the most influential climate variability on Earth, with cold (La Niña) and warm (El Niño) anomalous states emerging in the equatorial Pacific Ocean and altering weather and climate on a global scale through atmospheric teleconnections (Lau 1997; Alexander et al. 2002; McPhaden et al. 2006; Zhong et al. 2026). After the 1990s, El Niño events with anomalous sea surface temperature (SST) warming concentrated over the central Pacific have experienced a notable increase in occurrence. This distinct event has been referred to as "El Niño Modoki", "Date line El Niño", "warm pool El Niño", or "Central Pacific (CP) El Niño" (Larkin and Harrison 2005; Ashok et al. 2007; Kao and Yu 2009; Kug et al. 2009; Yeh et al. 2011; Yu and Kim 2013). The spatial and temporal characteristics, physical mechanisms, and climate impacts of the two types of El Niño events are quite different (Barnston et al. 2012; Clarke 2014; Yeh et al. 2015; Hu and Fedorov 2018).

Previous studies have provided different explanations for the mechanisms of CP El Niño events. Ashok et al. (2007) suggested that the occurrence of CP El Niño may be primarily driven by the weakening of the tropical Pacific trade

✉ Ruiqiang Ding
drq@bnu.edu.cn

1 State Key Laboratory of Earth Surface Processes and Disaster Risk Reduction (ESPDRR), Beijing Normal University, Beijing, China

2 Key Laboratory of Environmental Change and Natural Disasters of Chinese Ministry of Education, Beijing Normal University, Beijing, China

3 Frontiers Science Center for Deep Ocean Multispheres and Earth System (FDOMES)/Key Laboratory of Physical Oceanography/Institute for Advanced Ocean Studies, Ocean University of China, Qingdao, China

4 Qinghai Provincial Key Laboratory of Plateau Climate Change and Corresponding Ecological and Environmental Effects, Qinghai Institute of Technology, Xining 810016, China

5 Department of Atmospheric Sciences, School of Ecology and Environmental Science, Qinghai Institute of Technology, Xining 810016, China

winds. The weakened trade winds lead to a deepening of the tropical eastern Pacific thermocline, which results in fewer anomalous SST in the tropical eastern Pacific. Xie and Jin (2018) demonstrated that zonal advective (thermocline) feedback is more responsible for CP (EP) El Niño. Yeh et al. (2009) found that under global warming scenarios, the tropical Pacific thermocline becomes flattened and the east–west gradient of thermocline depth is reduced, which tends to enhance the zonal advective feedback in the central Pacific and therefore favors CP El Niño. Xu et al. (2012) highlighted that the interdecadal variability of subsurface ocean temperature in the equatorial Pacific is an important contributor to CP El Niño occurrence. Chen et al. (2015) suggested that the westerly wind bursts (WWBs) could influence the diversity of El Niño events, and the intensified (weakened) WWBs contribute to the development of EP (CP) El Niño events via the synergistic impacts of equatorial wave dynamics and surface warm-water advection.

Outside the tropical Pacific, recent studies recognized that North Tropical Atlantic (NTA) SST may be a precursor signal for CP El Niño events (Dommenget et al. 2006; Rodríguez-Fonseca et al. 2009; Jansen et al. 2009; Rong et al. 2010; Ham et al. 2013a; Li et al. 2015; Wang et al. 2017; Jiang and Li 2021; Ding et al. 2023; Tian et al. 2025). The NTA SST impacts the tropical Pacific primarily through two pathways: the Rossby wave process and the Kelvin wave process (Li et al. 2018). The Rossby wave process posits that the springtime NTA warming could trigger a low-level cyclonic flow to the west over the eastern Pacific as a Rossby wave response. On the western side of the anomalous cyclone, northerly anomalies strengthen the trade winds over the northeastern Pacific, resulting in a cold SST anomaly (SSTA) in the region. This cooling effect suppresses convection and forms a low-level anticyclonic flow to the west. On the southern side of the anticyclone, easterly anomalies act as a trigger for the CP-like La Niña (Ham et al. 2013b; Ham and Kug 2015). The Kelvin wave process supposes that spring NTA cold SST anomalies can induce surface westerly anomalies in the tropical Indian Ocean which superimpose on the background mean westerly wind in the northern Indian Ocean (NIO) and cool the SST there, which then induce westerly anomalies as a kelvin wave response to the east and ultimately influence the tropical Pacific SST (Rong et al. 2010; Yu et al. 2015a, b).

The studies presented above mainly focus on the role of the NTA SST in the occurrence of CP El Niño events. In this study, we provide further evidence that both the atmospheric and oceanic forcings over the North Atlantic play an important role in the occurrence of CP El Niño. Our results highlight the unique role of the Atlantic forcings in generating CP El Niño. Moreover, recent evidence suggests that Atlantic air-sea signals underwent a pronounced interdecadal change around the early 1990s. Ding et al. (2023) demonstrated that the relationship between the NTA SST and ENSO strengthened significantly after the early 1990s, owing to a transition of the North Atlantic Oscillation (NAO) toward a more positive phase. This interdecadal strengthening coincides with the increased occurrence of CP El Niño events after the 1990s, suggesting a potential linkage between the two. However, the physical processes through which strengthened Atlantic air–sea signals contribute to the increased occurrence of CP El Niño events remain unclear. In this study, we provide further evidence that Atlantic air-sea signals play an important role in the occurrence of CP El Niño. The remainder of this paper is organized as follows. Section 2 describes the datasets, methods, and climate indices used in this study. Section 3 provides evidence of the strengthened correlation between Atlantic forcing and CP El Niño events since the 1990s and identifies the crucial process that distinguishes between the two types of El Niño events as originating from the Atlantic. Our conclusions are summarized and discussed in Sect. 4.

2 Data and methods

2.1 Datasets

This study uses three observational datasets: (1) monthly mean SST data from the Hadley Centre Global Sea Ice and Sea Surface Temperature (HadISST), with a resolution of $1° \times 1°$, for the period 1950–2024 (Rayner et al. 2003); (2) monthly mean wind, sea level pressure (SLP), geopotential heights, net shortwave radiation flux, net longwave radiation flux, net sensible heat flux, net latent heat flux data from the National Centers for the Environment Prediction and the National Center for Atmospheric Research (NCEP-NCAR) reanalysis 1 Dataset, with a resolution of $2.5° \times 2.5°$, for the period 1950–2024 (Kalnay et al. 1996); (3) monthly mean subsurface ocean temperature, circulation, and surface wind stress data from the Global Ocean Data Assimilation System for the period 1980–2024 (Behringer et al. 1998). All monthly anomalies in this study are calculated by removing the average seasonal cycle from 1991 to 2020 and then removing the long-term linear trend by using least squares.

2.2 Indices

The NTA SST index (NTAI) is defined as the average of SSTA over the northern tropical Atlantic (0°–15°N, 90°W–20°E) (Ham et al. 2013b). The NAO index is defined as the principal component (PC) time series of the first empirical orthogonal function (EOF) of SLP anomalies over the northern Atlantic region (20°–80°N, 90°W–40°E)

(Xie and Tanimoto 1998). The Victoria mode (VM) index is defined as the second EOF of monthly SST anomalies over the North Pacific (120°E–150°W, 20°–60°N) (Bond et al. 2003). All climate indices used in this study were standardized prior to the analyses.

The intensity of CP El Niño can usually be represented by the Niño4 index, defined as the area average of SSTA over the equatorial central Pacific region (5°S–5°N, 160°E–150°W). In addition, three additional indices for CP El Niño are also used, including El Niño Modoki index (EMI), Niño Warm Pool (NWP) index, and CP index. Firstly, EMI is defined as follows:

$$\mathrm{EMI} = [\mathrm{SSTA}]_{\mathrm{A}} - 0.5^{*}[\mathrm{SSTA}]_{\mathrm{B}} - 0.5^{*}[\mathrm{SSTA}]_{\mathrm{c}} \tag{1}$$

where $[\mathrm{SSTA}]_{\mathrm{A}}$, $[\mathrm{SSTA}]_{\mathrm{B}}$ and $[\mathrm{SSTA}]_{\mathrm{c}}$ represent the area-averaged SSTA over region A (165°E–140°W, 10°S–10°N), B (110°W–70°W, 15°S–5°N), and C (125°E–145°E, 10°S–20°N) (Ashok et al. 2007). In addition, the NWP index is defined based on Niño3 and Niño4 as follows:

$$\begin{cases} \mathrm{NCT} = \mathrm{Ni\ no3} - \alpha \mathrm{Ni\ no4} \\ \mathrm{NWP} = \mathrm{Ni\ no4} - \alpha \mathrm{Ni\ no3} \end{cases}, \quad \alpha = \begin{cases} 2/5, & \mathrm{Ni\ no3}^{*}\mathrm{Ni\ no4} > 0 \\ 0, & \mathrm{otherwise} \end{cases} \tag{2}$$

where Niño Cold Tongue (NCT) index represents the intensity of EP El Niño (Ren and Jin 2011). The Niño3 index is defined as the area average of SSTA over the equatorial Pacific region (5°S–5°N, 150°–90°W). The CP index is defined as the PC time series of the leading EOF of SST anomalies over the equatorial Pacific region (20°S–20°N, 120°E–80°W), removed Niño1+2 by linear regression (Kao and Yu 2009).

2.3 Methods

The mixed-layer heat budget is calculated as follows (Huang et al. 2012):

$$\frac{\partial T'}{\partial t} = -\frac{u'\partial \overline{T}}{\partial x} - \frac{\overline{u}\partial T'}{\partial x} - \frac{u'\partial T'}{\partial x} - \frac{v'\partial \overline{T}}{\partial y} - \frac{\overline{v}\partial T'}{\partial y} - \frac{v'\partial T'}{\partial y} - \frac{w'\partial \overline{T}}{\partial z} - \frac{\overline{w}\partial T'}{\partial z} - \frac{w'\partial T'}{\partial z} + Q' + R \tag{3}$$

where T, Q, and R denote the mix-layer temperature, thermal forcing, and residue; u, v, and w denote the zonal, meridional, and vertical current. The overbar denotes the climatological seasonal mean, whereas the prime denotes the anomaly relative to the climatological seasonal mean.

The statistical significance was determined using a two-tailed Student's t-test. We employ statistical methods including correlation and composite analysis to examine whether the linkage between Atlantic forcings and CP El Niño is statistically significant. The effective number (N^{*}) of degrees of freedom is calculated as follows by (Bretherton et al. 1999):

$$N^{*} \approx N\frac{1 - R_x R_y}{1 + R_x R_y} \tag{4}$$

where N is the sample time series size and R_x, R_y represent the lag-one autocorrelations of variables x and y.

3 Results

3.1 Relationships between the Atlantic air-sea signals and CP El Niño variability

To investigate the reasons for the increase in CP El Niño events after the 1990s, it is necessary to identify the air-sea signals that are most relevant to CP El Niño variability. Figure 1 illustrates the correlation patterns of the previous boreal winter (D-1JF0) SLP and springtime (MAM0) SST with the subsequent winter (D0JF1) Niño4 index for the periods 1955–1989 (hereafter P1) and 1990–2024 (hereafter P2), respectively. During P1, the correlation pattern exhibits a negative NAO-like dipole pattern in the North Atlantic (Fig. 1a). In contrast, during P2, the SLP signal reveals a stronger Azores High (Fig. 1b). Meanwhile, significant North Pacific Oscillation (NPO)-related atmospheric signals are evident over the North Pacific in both P1 and P2 (Fig. 1a,b). As for SST signals, both periods exhibit significant VM in the Pacific region (Bond et al. 2003; Ding et al. 2015a,b). However, the significant North Atlantic Tripole (NAT) pattern emerges exclusively during P2, coinciding with cold SST anomalies in the NTA region (Fig. 1d, e). The correlated changes in SLP and SST from P1 to P2 are characterized by a positive phase of the NAO and a negative NTA mode in the North Atlantic (Fig. 1c, f), respectively, while there are no significant differences between the two periods in the Pacific region. These results indicate that the relationship between Atlantic air–sea signals and CP El Niño variability became significantly stronger after the 1990s. Similar results are also obtained when three alternative indices for representing CP El Niño variability are analyzed (Fig. 2).

Furthermore, the mean state differences in SLP and SST anomalies between P1 and P2 also reveal this shift in air-sea signals during these two periods, which is consistent with the correlated changes in SLP and SST fields mentioned earlier. The mean SLP difference (P2 minus P1) is characterized by a negative phase of the NAO (Fig. 3a). Simultaneously, the mean SST difference (P2 minus P1) features a NAT-like

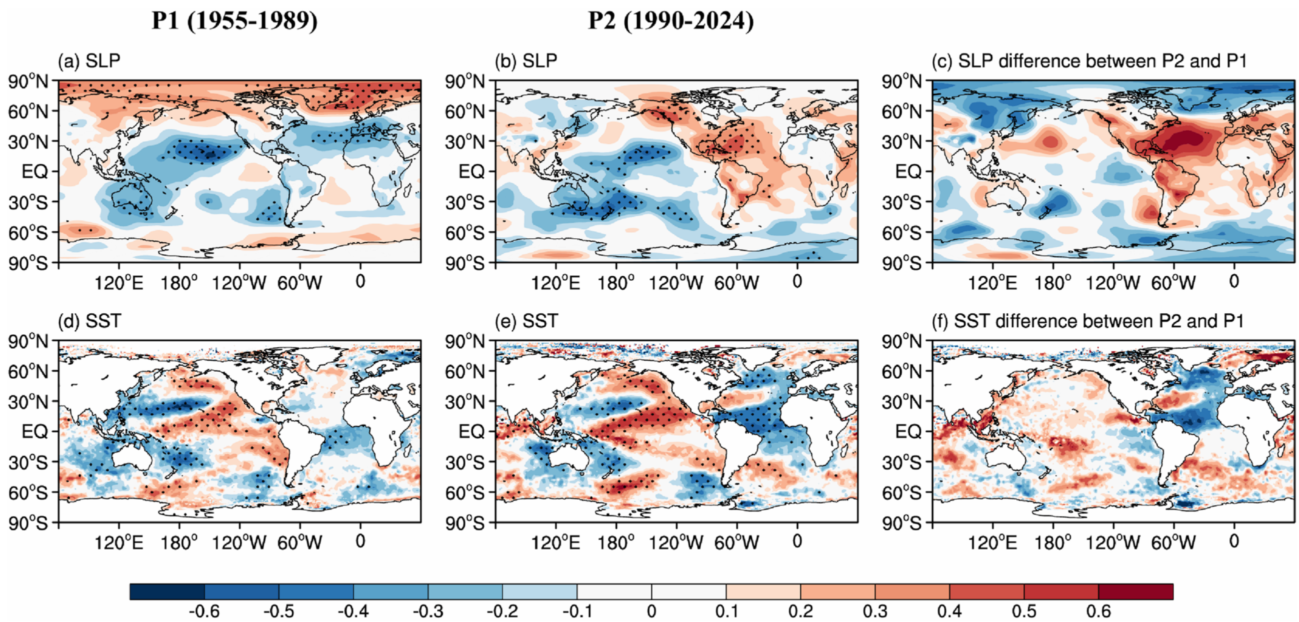

Fig. 1 **a, b** Correlations between the subsequent winter (D0JF1) Niño4 index and previous winter (D-1JF0) SLP (shading, hPa) anomalies during 1955–1989 (P1) **a** and 1990–2024 (P2) **b**, and **c** their difference, respectively. **d, e** Correlations between the subsequent winter (D0JF1) Niño4 index and the boreal spring (MAM0) SST (shading, °C) anomalies during P1 **d** and P2 **e**, and **f** their difference, respectively. In **a**, **b**, **d**, **e**, stipples indicate correlations significant at the 95% confidence level. Here, the winter (spring) season was chosen because it is the primary peak season of the NAO (NTA SST)

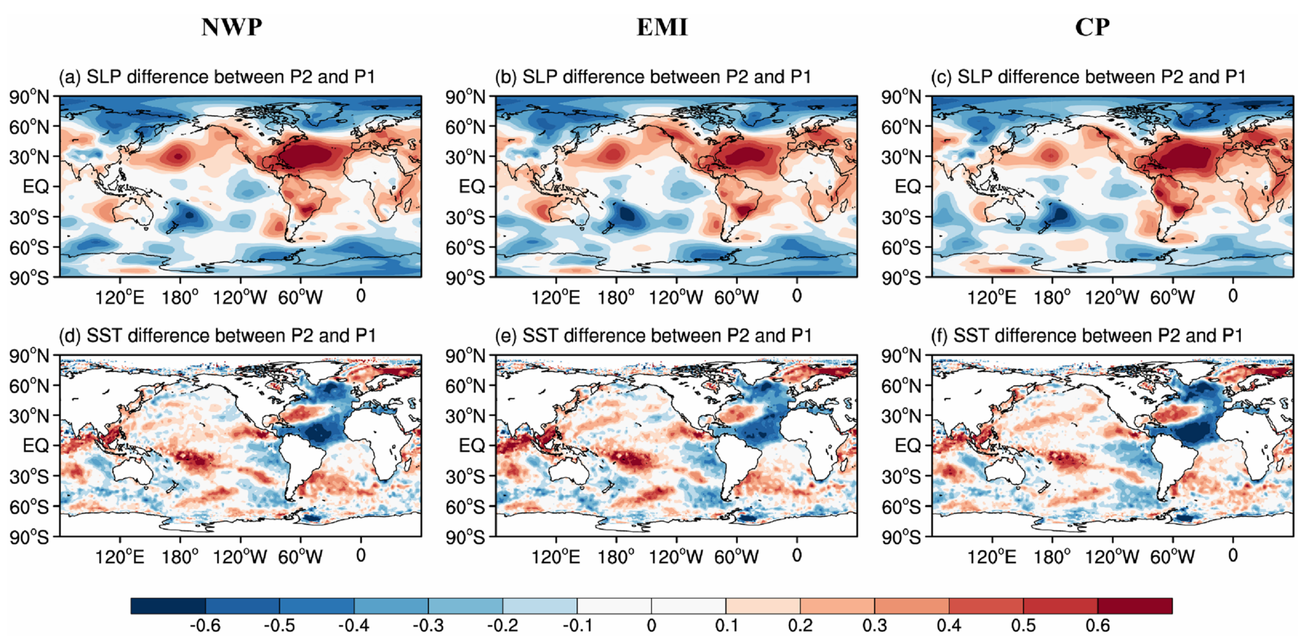

Fig. 2 **a**–**c** As in Fig. 1. **c**, but for the subsequent winter (D0JF1) NWP (**a**), EMI (**b**), CP index (**c**). **d**–**f** As in Fig. 1. **f**, but for the subsequent winter (D0JF1) NWP (**d**), EMI (**e**), CP index (**f**)

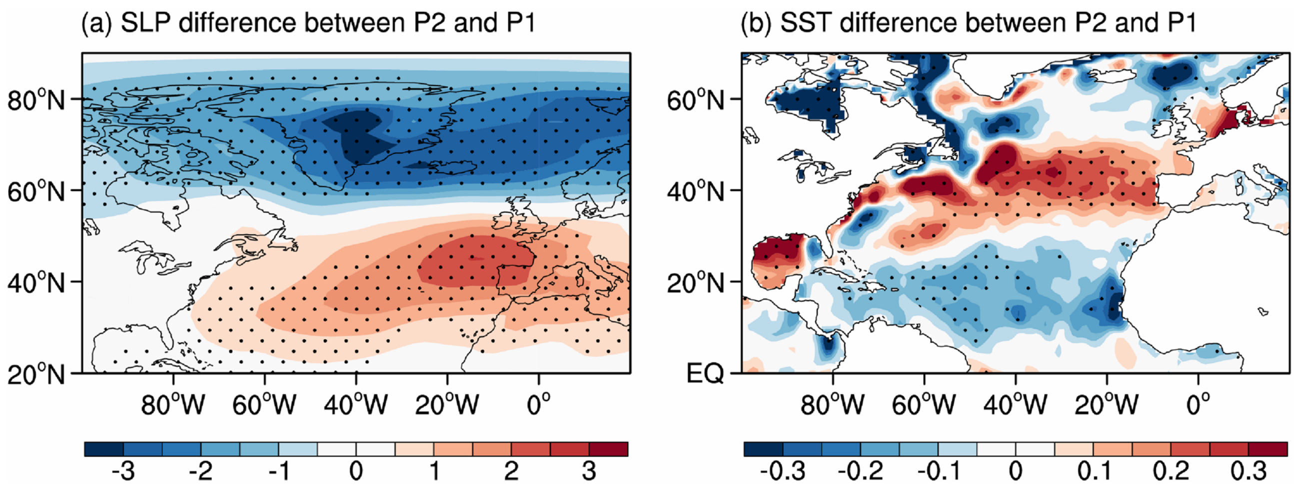

Fig. 3 Differences differences of the previous boreal winter (D-1JF0) SLP (shading, hPa) (**a**) and spring (MAM0) SST (shading, °C) (**b**) anomalies between 1990 and 2024 (P2) and 1955–1989 (P1). Stipples indicate SLP and SST anomalies significant at the 95% confidence level

Table 1 CP and EP El Niño events after the 1990s

CP	EP
1994/95	1991/92
2002/03	1997/98
2004/05	2006/07
2009/10	2015/16
2014/15	
2018/19	

SST anomaly pattern, corresponding to cold SST anomalies in the NTA region (Fig. 3b). These results further indicate that the Atlantic air–sea signals are shifting in a direction conducive to the occurrence of CP El Niño after the 1990s, which is consistent with the period since the 1990s when CP El Niño events have occurred frequently.

3.2 CP El Niño events key processes

Before investigating the mechanisms through which the Atlantic air-sea signals influence CP El Niño, we first need to delve deeply into the distinct key processes contributing to the CP El Niño events after the 1990s. According to NOAA CPC data, there have been a total of 10 El Niño events since the 1990s, with 6 classified as CP El Niño events and 4 as EP El Niño events (Table 1). The classification between CP and EP events is based on the index defined by Ren and Jin (2011). We also conduct composite analyses with other CP indices, and different CP classification choices have little influence on our following results.

To elucidate the primary disparities in the development and formation processes between CP El Niño and EP El Niño events, we first focus on the preconditioning phase. This stage spans the boreal winter one year prior to El Niño maturity (D-1JF0) to boreal spring of the El Niño developing year (MAM0). After the 1990s, for CP El Niño events, the 200 hPa height field displays a pronounced dipole pattern over the North Atlantic region (Fig. 4a, b). In contrast, EP El Niño events do not exhibit the North Atlantic dipole mode (Fig. 4c, d). The disparities in SSTA between the two types of El Niño events are markedly more pronounced. For CP El Niño events, there is a significant negative NTA mode in boreal spring (MAM0), with the entire Atlantic Ocean exhibiting a NAT pattern (Fig. 4f). In contrast, EP El Niño events do not exhibit significant SST signals in the North Atlantic, but rather a VM pattern in the Pacific (Fig. 4g, h).

Two types of El Niño events exhibit different air-sea signals and circulation patterns, which can directly influence the initial warming processes that lead to the diversity of El Niño events. For CP El Niño events, the initial SST warming begins in the region (5°N–20°N, 150°W–120°W) during spring (Fig. 4f). Meanwhile, there is anomalous upward motion within a small range near 150°W, which establishes during DJF and is further intensified due to abnormal warming of SST in this region during MAM (Fig. 4i, j). Compared with CP El Niño events, EP El Niño events exhibit a VM signal in the preceding winter, with significant warm SST anomalies in the central equatorial Pacific (Fig. 4g, h). Simultaneously, EP El Niño events are characterized by strong upward motion within the range of 150°E–150°W (Fig. 4l). The initial warming locations of the two types of El Niño events are close to each other, but there are fundamental differences in their seasonal evolution characteristics and precursor signals.

To further discern the mechanism underlying the initial warming that leads to the diversity of El Niño events, we select the region (5–20°N, 150°W–120°W) as the critical initial warming area and analyze the evolution of various terms in the SST tendency equation (see Methods). For CP

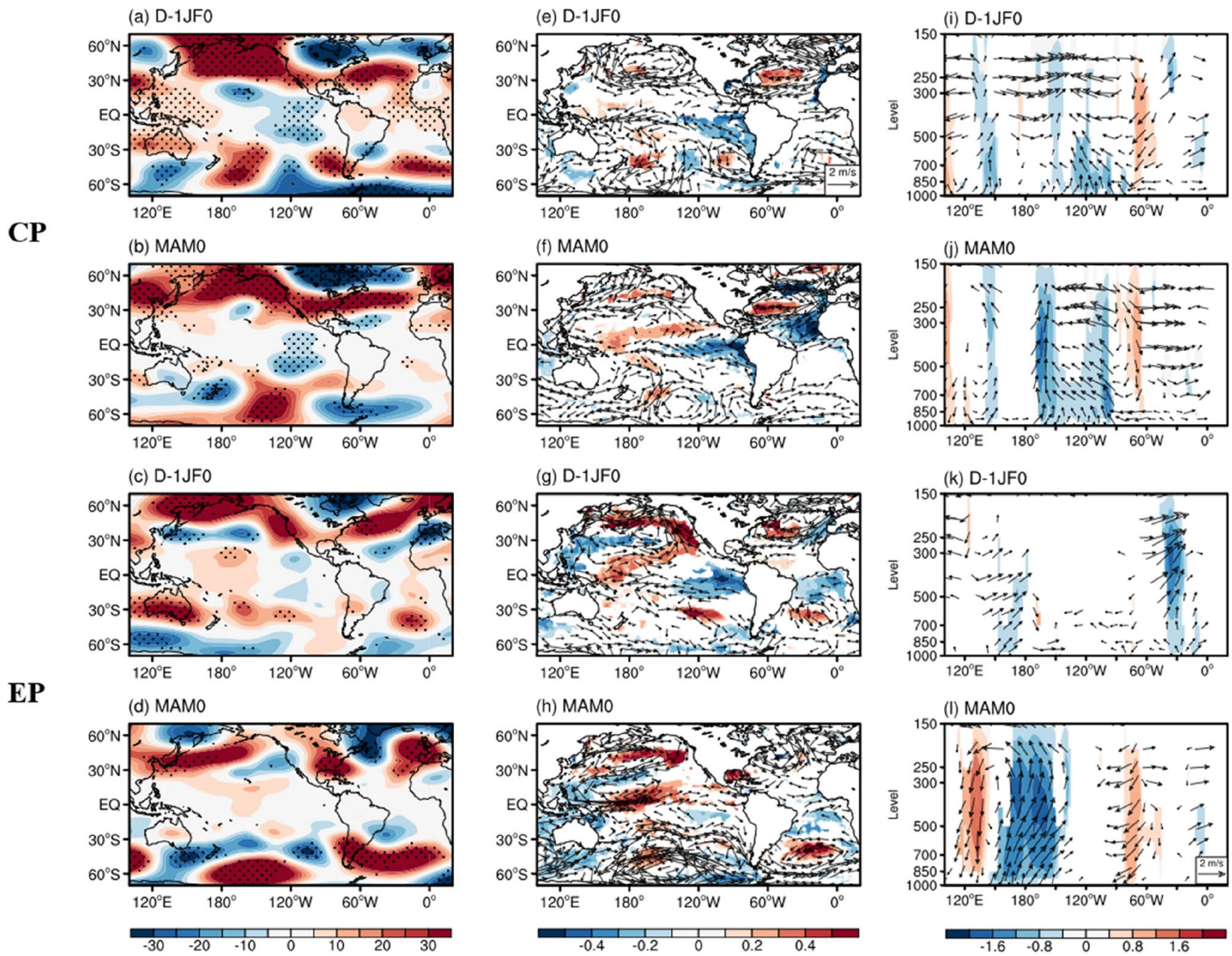

Fig. 4 **a**, **b** Composite seasonal averages of 200 hPa height (shading, m) anomalies from D-1JF0 (**a**) to MAM0 (**b**) for six CP El Niño events listed in Table 1. **c**, **d** As in (**a**, **b**), but for four EP El Niño events listed in Table 1. **e**–**h** As in **a**–**d**, but for SST (shading, °C) and surface wind (vectors, m s^{-1}) anomalies. **i**–**l** As in **a**–**d**, but for vertical atmospheric velocity (averaged between 5°N and 20°N; shading; Pa s^{-1}) and equatorial atmospheric vector (zonal wind and vertical velocity; vectors; m s^{-1}). In **a**–**d**, stipples indicate height anomalies significant at the 95% confidence level. In **e**–**l**, only anomalies significant at the 95% confidence level are shown

El Niño events, the SST tendency term ($\frac{\partial T'}{\partial t}$) is closest to the thermal term ($Q\prime$), indicating that the thermal term is the dominant factor for the initial warming (Fig. 5a, b). Specifically, there is warming from pre-winter to spring within the 150°W–120°W range (Fig. 5a). To further investigate the contributors to SST warming, we dissected the thermal term in the SST tendency equation into its components, including shortwave radiation (SWR), longwave radiation (LWR), latent heat flux (LHF), and sensible heat flux (SHF). Among these components, the LHF anomaly is the most prominent contributor to SST warming in the critical warming area (Fig. 5d). The initial warming is mainly manifested as abnormal LHF caused by abnormal surface winds, indicating that the surface wind forcing contributes significantly to the initial warming in the critical area of the CP El Niño event during spring (Fig. 4f). The southwesterly winds on the west side of the NTA-induced anticyclonic circulation above the critical warming area, reduce the northeasterly trade winds, weaken surface winds, and generating positive wind-induced LHF components. According to the wind–evaporation–SST (WES) feedback mechanism, this forms the initial SST warming (Ham et al. 2013b; Jiang and Li 2021). Regarding EP El Niño events, SST warming in this region is not particularly pronounced during the winter-spring season and may originate from the inherent warm SST signals within the Pacific itself, rather than being triggered by abnormal atmospheric circulation in the previous winter and spring (Fig. 5g, h).

The above analyses reveal the different initial warming mechanisms of the two types of El Niño events during the preconditioning phase of El Niño. This section further investigates the anomalous temperature evolution characteristics

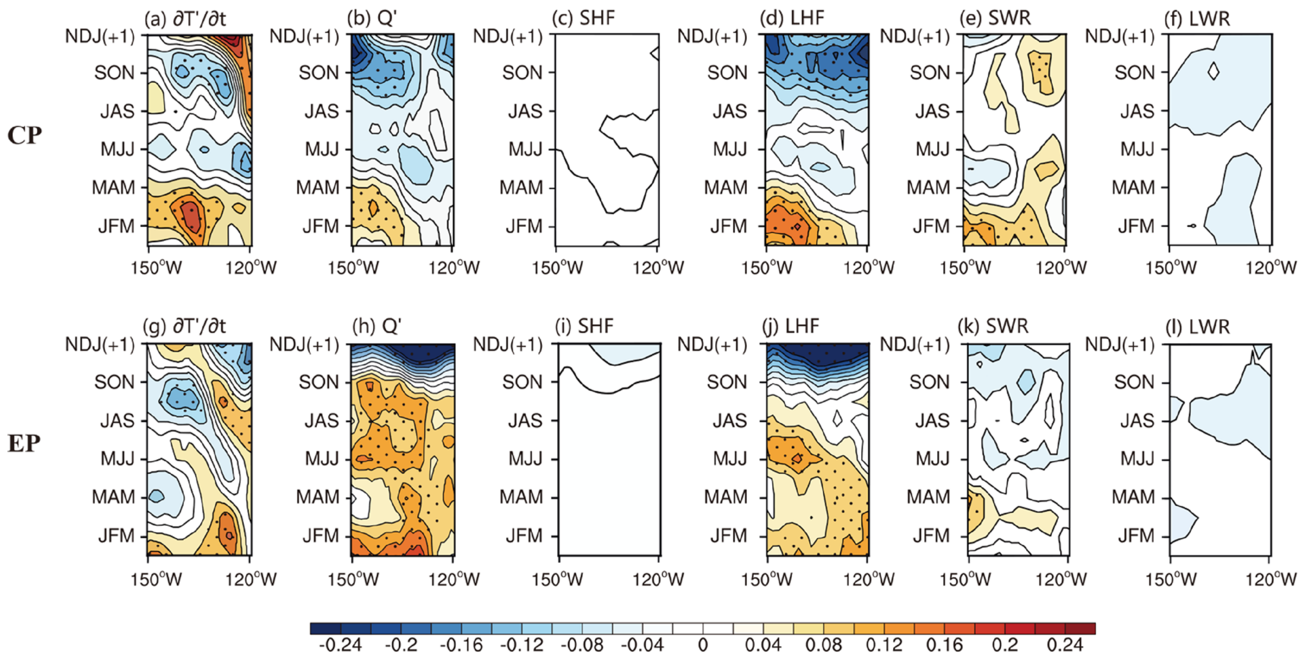

Fig. 5 **a**–**f** The longitude-time plot of 5°N–20°N averaged **a** mixed layer temperature anomaly tendency ($\frac{\partial T'}{\partial t}$) and **b** thermal forcing (Q′), **c** sensible heat flux (SHF), **d** latent heat flux (LHF), (**e**) shortwave radiation flux (SWR), **f** longwave radiation flux (LWR) anomalies from JFM0 to NDJ (+1) for six CP El Niño events listed in Table 1. **g**–**l** As in **a**–**f** but for four EP El Niño events listed in Table 1. Stipples indicate anomalies significant at the 95% confidence level

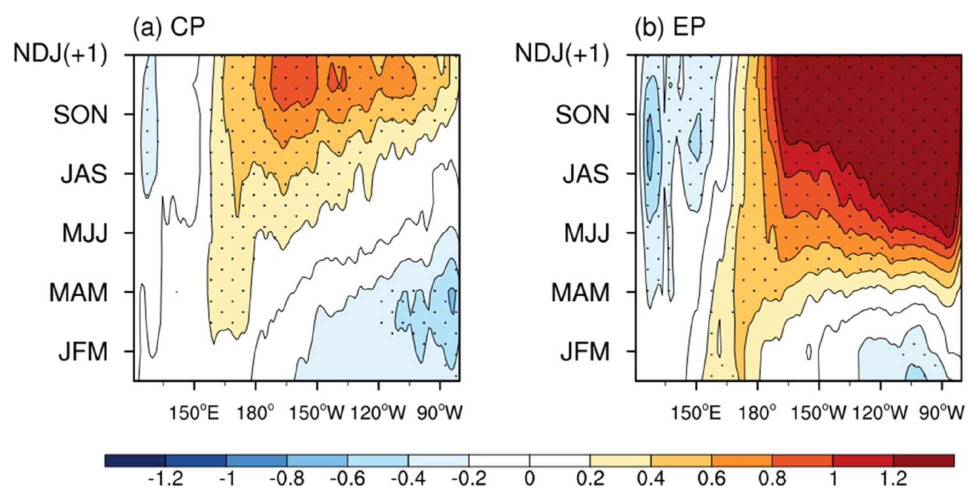

Fig. 6 The longitude-time plot of equatorial Pacific (averaged between 5°S–5°N) SST anomalies (shading, °C) from JFM0 to NDJ (+1) for six CP (**a**) and four EP (**b**) El Niño events listed in Table 1. Stipples indicate anomalies significant at the 95% confidence level

and key processes of the two types of El Niño events during the development phase of the El Niño. Following the initial warming in the winter-spring period, both CP and EP El Niño events exhibit significant differences in SST evolution and atmospheric circulation during the summer and autumn seasons. For both CP and EP El Niño events, SST warming initially occurs in the central Pacific region. However, there is a distinct divergence in the subsequent evolution of SST and circulation anomalies (Figs. 6 and 7). For CP El Niño events, the SST warming remains confined to the central Pacific region (Figs. 6a and 7a–d). In contrast, for EP El Niño events, the SST warming progresses with the seasons and propagates eastward into the eastern Pacific (Figs. 6b and 7e–h). This difference in the spatial distribution of SST warming propagation in the equatorial Pacific determines the ultimate forms of these two distinct types of El Niño events.

To explore the mechanisms underlying the temperature anomaly evolution of the two types of El Niño events, we once again employed the SST tendency equation approach to diagnose the SST tendency characteristics of these two types of El Niño events in the equatorial region (Fig. 8). The results show that warming occurred mainly within the range of 150°W–90°W (Fig. 8a, d). Previous studies have

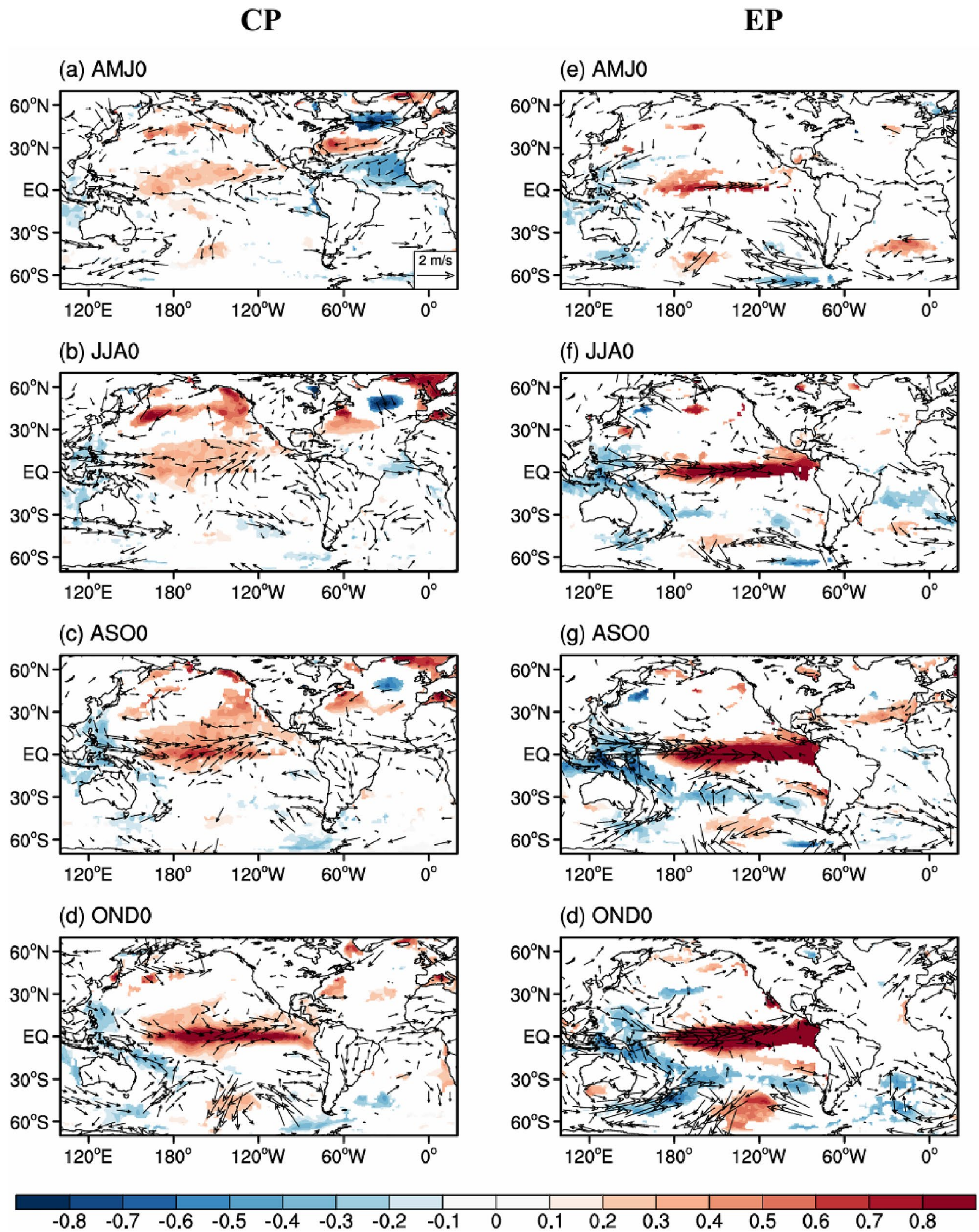

Fig. 7 **a**–**d** Composite seasonal evolution of SST (shading, °C) and surface wind (vectors, m s^{-1}) anomalies for AMJ0 (**a**), JJA0 (**b**), ASO0 (**c**), and OND0 (**d**) seasons for six CP El Niño events listed in Table 1. **e**–**h** As in **a**–**d**, but for four EP El Niño events listed in Table 1. Only anomalies significant at the 95% confidence level are shown

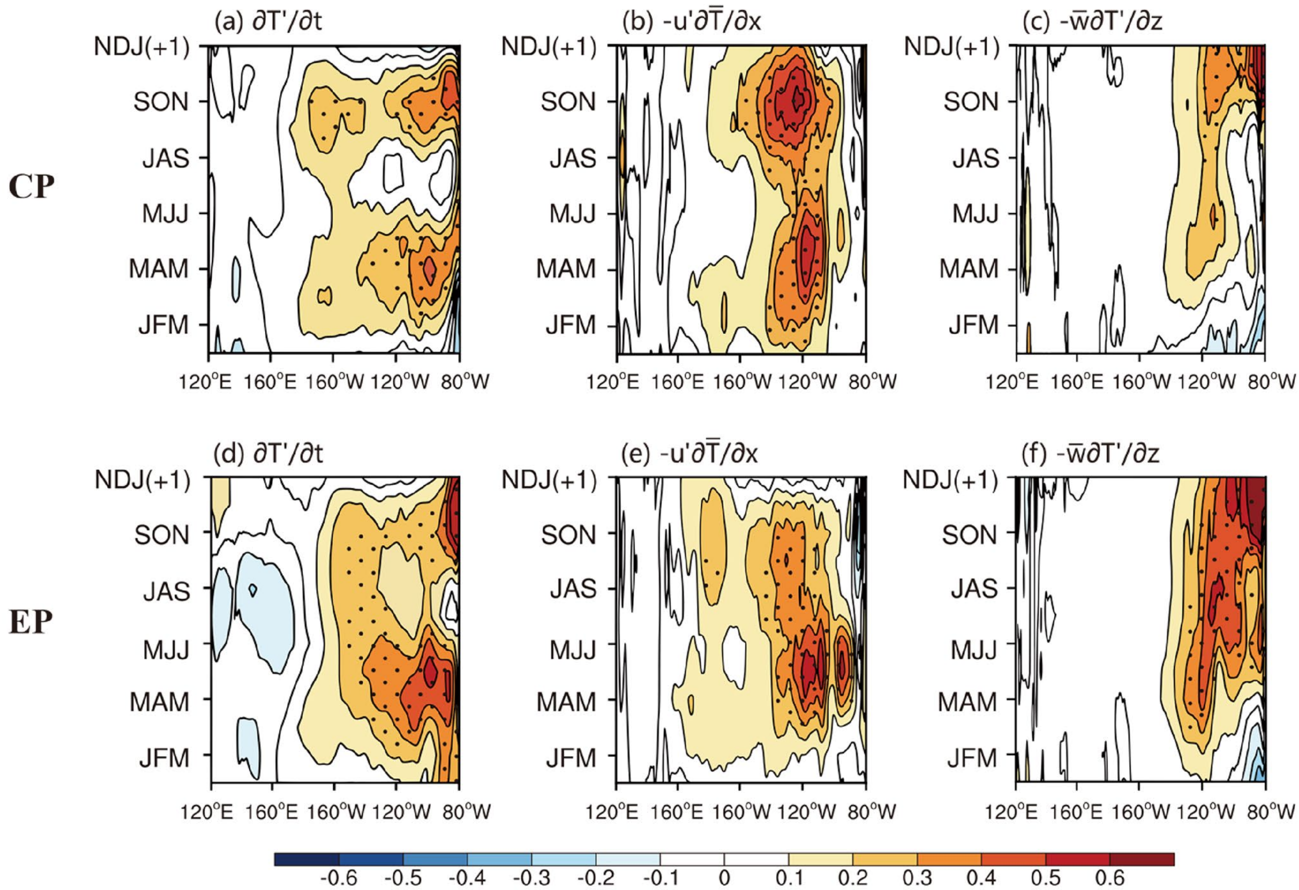

Fig. 8 **a**–**c** The longitude-time plot of 5°S–5°N averaged **a** mixed layer temperature anomaly tendency ($\frac{\partial T'}{\partial t}$) and **b** anomalous zonal advection ($-\frac{u'\partial \overline{T}}{\partial x}$), **c** thermocline feedback ($-\frac{\overline{w}\partial T'}{\partial z}$) from JFM0 to NDJ (+1) for six CP El Niño events listed in Table 1. **d**–**f** As in **a**–**c**, but for four EP El Niño events listed in Table 1. Stipples indicate anomalies significant at the 95% confidence level

suggested that zonal advection feedback is the most crucial mechanism driving the development of CP El Niño events, while the development of EP El Niño events relies on the combined effects of zonal advection and thermocline feedback (Kug et al. 2009). Zonal advection feedback dominates the development of both types of events during spring and summer. Specifically, the zonal advective feedback of EP El Niño events results in a significant positive temperature tendency in the equatorial eastern Pacific (Fig. 8e). In contrast, the zonal advective feedback of CP El Niño events is restricted to the central Pacific region (Fig. 8b). In addition, for CP El Niño events, the thermocline feedback is characterized by weaker intensity and continuity (Fig. 8c), indicating that continuous zonal advection feedback dominates from spring to winter as the largest contributor to CP El Niño events. In contrast, EP El Niño events exhibit a continuous seasonal intensification in the eastern equatorial Pacific, which persists through autumn and winter (Fig. 8f). The positive zonal advection feedback and sustained positive thermocline feedback in the eastern Pacific heat the eastern Pacific in spring and summer, and the warm SST develops eastward, ultimately forming the EP El Niño event (Figs. 6b and 8e–f). These diagnostic results highlight that the timing and spatial distribution of the thermocline feedback and zonal advection feedback play distinct roles in determining the diversity of El Niño events.

The differences in zonal advection feedback between CP and EP El Niño events primarily arise from disparities in the surface wind field distribution, highlighting the pivotal role of wind anomalies. For CP El Niño events, there is a persistent easterly anomaly in the eastern equatorial Pacific from spring to winter (Fig. 9). The presence of this easterly anomaly suppresses the eastward propagation of zonal advection feedback, thereby confining the effect of the zonal advection feedback to the central Pacific region (Fig. 8b). During the development phase of the El Niño, although westerly anomalies strengthen during both types of El Niño events, the westerly anomalies in EP El Niño events are stronger and their influence extends closer to the eastern equatorial Pacific region (Fig. 9b–c). This facilitates the action of zonal advection feedback in the eastern equatorial Pacific, leading to SST warming in that region. Given the persistent

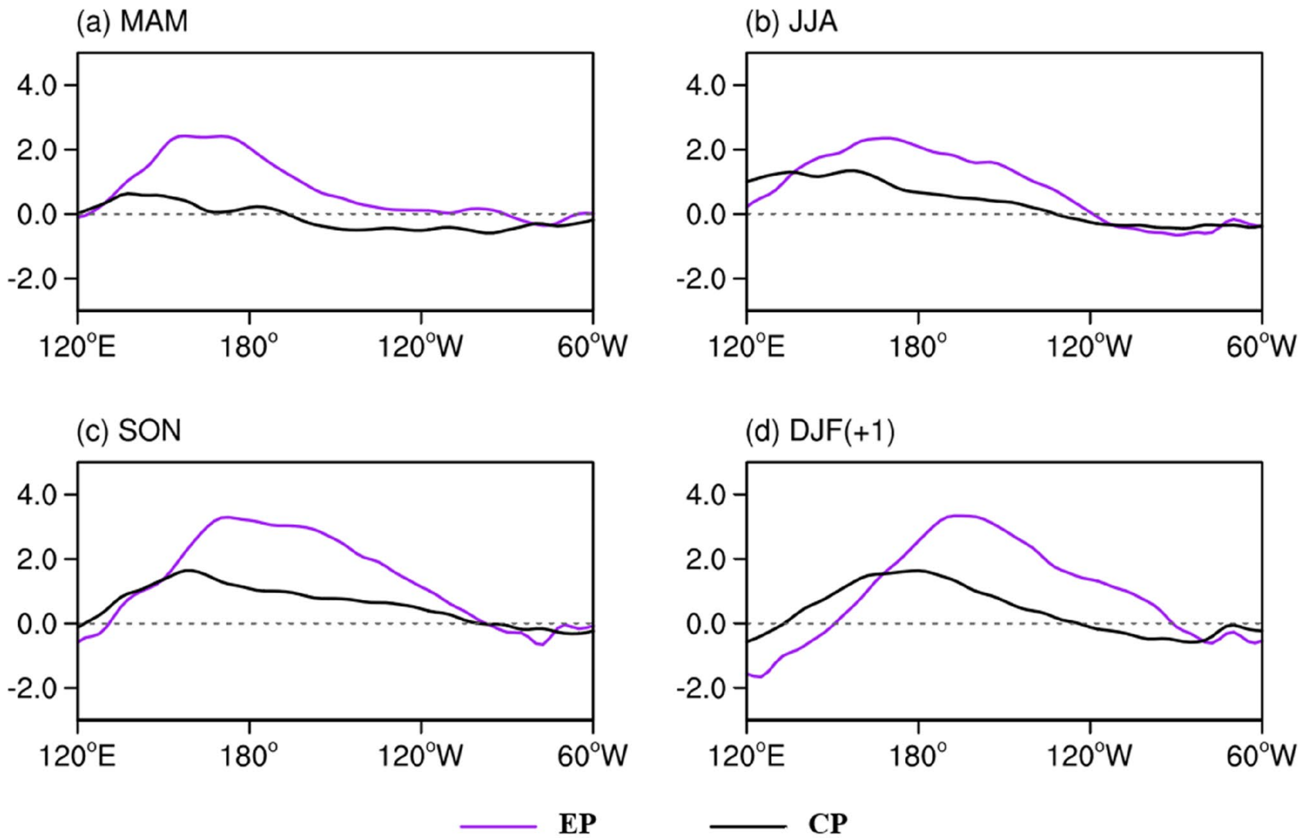

Fig. 9 **a**–**d** Composite seasonal averages of equatorial (10°S–10°N) averaged latitudinal winds anomalies for MAM0 (**a**), JJA0 (**b**), SON0 (**c**), and DJF (+1) (**d**) seasons for the six CP (black line) and four EP (purple line) El Niño events listed in Table 1. Negative value indicates represent anomalous easterly

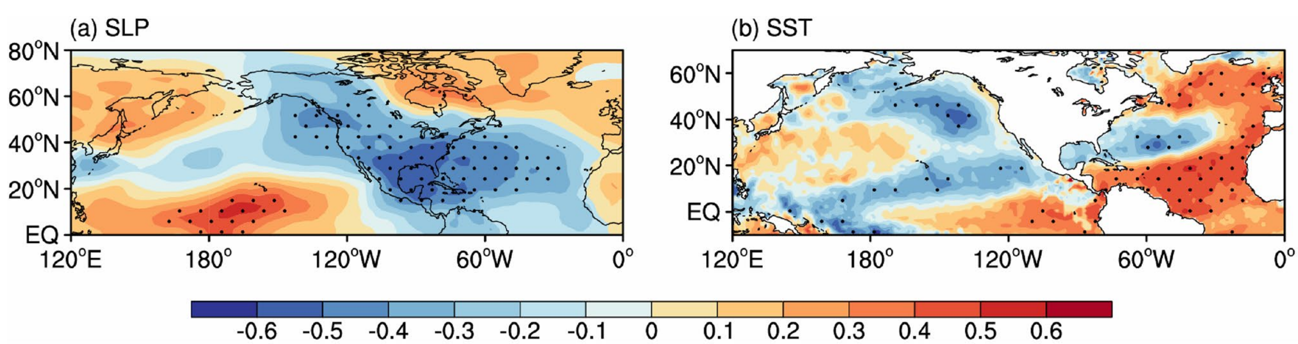

Fig. 10 Correlations between the previous boreal winter (D-1JF0) SLP (shading, hPa) (**a**) and spring (MAM0) SST (shading, °C) (**b**) anomalies, and spring (MAM0) latitudinal winds anomalies (averaged in 10°S–10°N, 150°W–60°W) during 1990–2024. Stipples indicate correlations significant at the 95% confidence level

easterly anomalies in the eastern Pacific, the dragging effect exerted by the wind field on seawater also affects the intensity and scope of thermocline feedback, further determining the diverse development patterns of El Niño events (Hu et al. 2016).

3.3 North Atlantic forcing mechanisms

The above comparative analysis of post-1990 CP and EP El Niño events has identified persistent equatorial eastern Pacific easterly anomalies as the vital process confining warm SST anomalies within the central Pacific (Fig. 9). Given the strengthened Atlantic–CP El Niño linkage after the 1990s shown in Sect. 3.1, we now examine whether these critical easterly wind anomalies are dynamically linked to Atlantic air–sea signals (Fig. 10). The anomalous SLP associated with the easterly anomalies exhibit a NAO-like north–south dipole pattern over the North Atlantic. In addition, the correlated pattern between the easterly anomalies and the SST field resembles the NAT SST pattern. These results indicate that springtime easterly anomalies are significantly associated with North Atlantic forcings, demonstrating the connection between the Atlantic air-sea signals and the key processes.

It has been well recognized that NAO can influence the relationship between NTA and ENSO events (Xie and Tanimoto 1998; Ding et al. 2023). The intensification of the NTA-ENSO relationship after the 1990s is closely associated with the phase transition of NAO. After the 1990s, the positive phase of the previous winter (D-1JF0) NAO induces pronounced atmospheric circulation anomalies over the North Atlantic. The strengthened Azores High and enhanced subtropical pressure gradient intensify the northeasterly trade winds over the NTA region. These wind anomalies increase surface evaporation and upward LHF, leading to ocean heat loss and cooling of the mixed layer. At the same time, enhanced wind stress promotes vertical mixing and entrainment of colder subsurface water, further reinforcing the surface cooling. Through the combined effects of LHF and ocean dynamical processes, negative SST anomalies develop over the NTA during the following spring (MAM0). Acting as a bridge, the NTA then transmits the Atlantic influence to the tropical Pacific circulation, thereby affecting the development of CP El Niño (Fig. 11). The unique role of Atlantic air-sea signals in key processes can be illustrated through the bridging function of the NTA.

Previous studies have highlighted that the existence of the VM in the Pacific Ocean facilitates the occurrence of CP El Niño events, underscoring the role of Pacific air-sea signals in triggering such events (Ding et al. 2015b). To verify the unique influence of Atlantic signals on CP El Niño, we use VM events as representatives of Pacific SST signals and NTA events as representatives of Atlantic SST signals. Specifically, we perform composite analyses on negative NTA events that occurred after the 1990s and compare these results with the composite fields obtained from positive VM events after excluding those with negative NTA events (Fig. 12). The NTA cooling can generate an anticyclonic Rossby wave over the subtropical eastern Pacific as a Gill-type Rossby-wave response during spring (Gill 1980), which produces an easterly anomaly on its eastern flank (Fig. 12a). Due to the persistent presence of easterly anomalies in the equatorial eastern Pacific (Fig. 13a), warm SST anomalies are ultimately confined to the central Pacific through zonal advection feedback during winter (Fig. 12c, d). By synthesizing positive VM events and excluding years with negative NTA events, we obtain the seasonal evolution of SST that more closely resembles the EP El Niño development process (Fig. 12e–h). There are no sustained easterly anomalies in the equatorial Pacific (Fig. 13b), and continuous strong westerly anomalies keep the warm SST moving eastward. This highlights the unique role of the Atlantic in CP El Niño events. In the absence of an Atlantic signal, the eastward development of warm SST is not blocked (Fig. 12h), even though the initial warming occurs in the Central Pacific (Fig. 12e). These results reveal that the key process originates from the NTA-induced easterly anomalies, thereby further confirming the unique role played by the anomalous Atlantic air-sea signals.

Finally, we compiled an event-by-event summary of the major signals related to Atlantic and Pacific precursors associated with the six CP El Niño events occurring after the 1990s (Table 2). Specifically, we inspected the previous winter NAO and spring NTA SST anomalies that jointly compose Atlantic air–sea forcing, alongside the VM and seasonal features of WWBs. Five of the six CP El Niño events (83%) featured the typical configuration of Atlantic air–sea signals with a positive winter NAO paired with negative spring NTA SST anomalies, indicating that such Atlantic air–sea interactions deliver the most recurrent large-scale contribution. Suppressed intense WWBs activity characterizes the development stage of all six post-1990 CP El Niño events, with no clustered strong WWBs sequences comparable to those closely linked to EP El Niño. Such weak WWB activity constitutes a favorable internal Pacific state conducive to central Pacific warming, yet this condition alone cannot generate the persistent equatorial eastern Pacific easterly barrier required to confine warm SST anomalies. The 2004/05 event was the only case lacking clear signatures of Atlantic air–sea forcing; despite the absence of intense WWBs, its central Pacific warming signal was relatively weak and short-lived, further highlighting the dominant and unique contribution of Atlantic air–sea interactions. By contrast, the 2014/15 event combined a positive VM with robust signals of Atlantic air–sea forcing, where Atlantic-related easterly anomalies remained the primary factor limiting eastward SST expansion despite the coexisting Pacific precursor. No CP event exhibits substantial stable central Pacific warming without coordinated signals of Atlantic air–sea forcing, even under suppressed WWBs. Overall, these event statistics suggest that Atlantic air–sea forcing provides the dominant, irreplaceable remote influence on post-1990 canonical CP El Niño variability, whereas the VM only modulates CP evolution when superimposed on Atlantic signals, and suppressed intense WWBs serve as a necessary but insufficient internal condition supporting stable central Pacific warming.

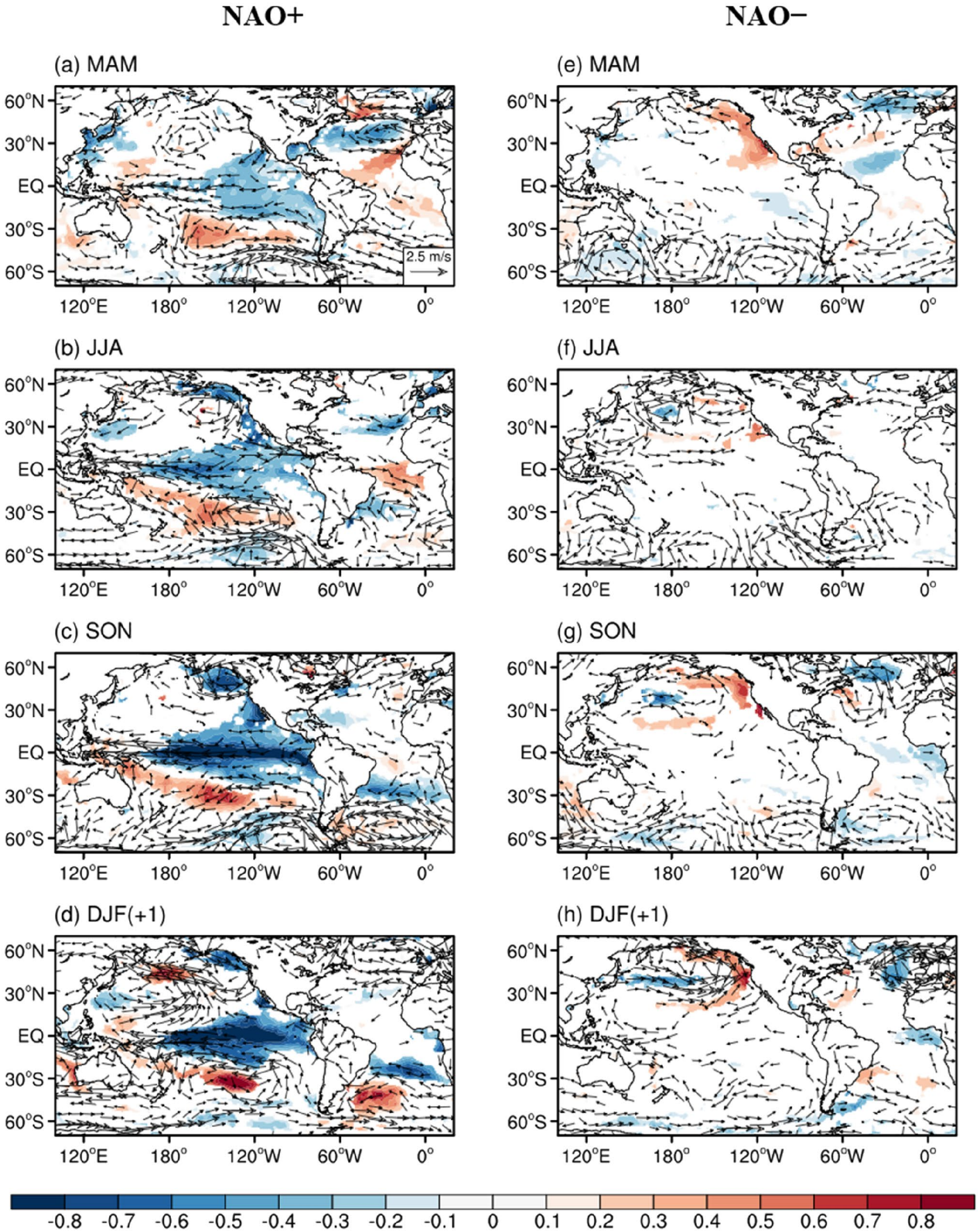

Fig. 11 **a**–**d** Composite seasonal evolution of SST (shading, °C) and surface wind (vectors, m s^{-1}) anomalies from MAM0 (**a**), JJA0 (**b**), SON0 (**c**), and DJF (+1) (**d**) seasons for the strongly positive NAO events (NAO+). **e**–**h** As in **a**–**d**, but for the strongly negative NAO events (NAO−). Only anomalies significant at the 95% confidence level are shown. One positive (or negative) NAO event is defined as a period when the NAO index anomaly is greater than 1 standard deviation (SD) or less than-1 SD

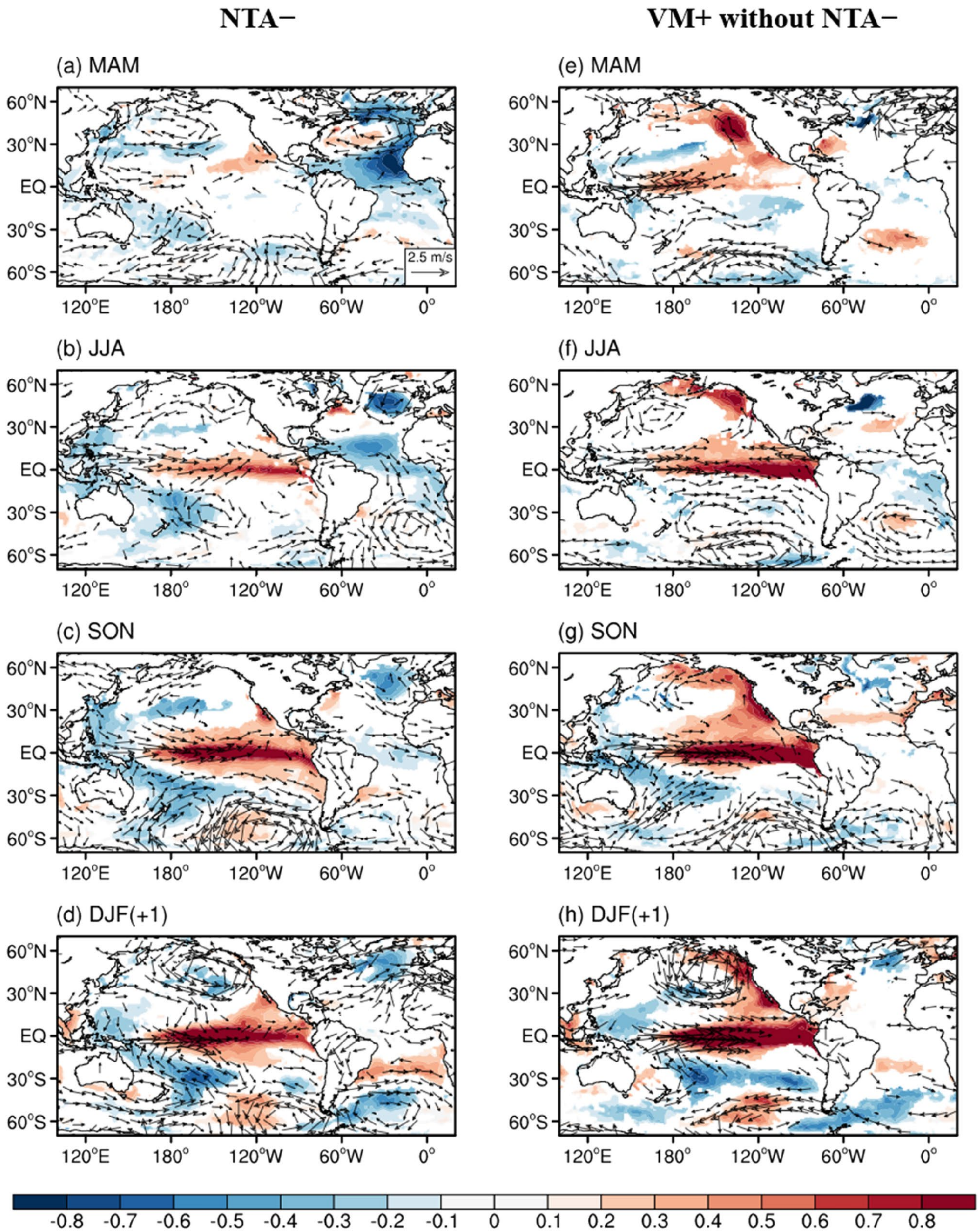

Fig. 12 **a**–**d** Composite seasonal evolution of SST (shading, °C) and surface wind (vectors, m s^{-1}) anomalies from MAM0 (**a**), JJA0 (**b**), SON0 (**c**), and DJF (+1) (**d**) seasons for the strongly negative NTA events (NTA−). **e**–**h** As in **a**–**d**, but for the strongly positive VM without negative NTA events (VM+without NTA−). Only anomalies significant at the 95% confidence level are shown. One positive VM event (negative NTA SST events) is defined as a period when the VM index (NTA index) anomaly is greater than (less than) 1 SD

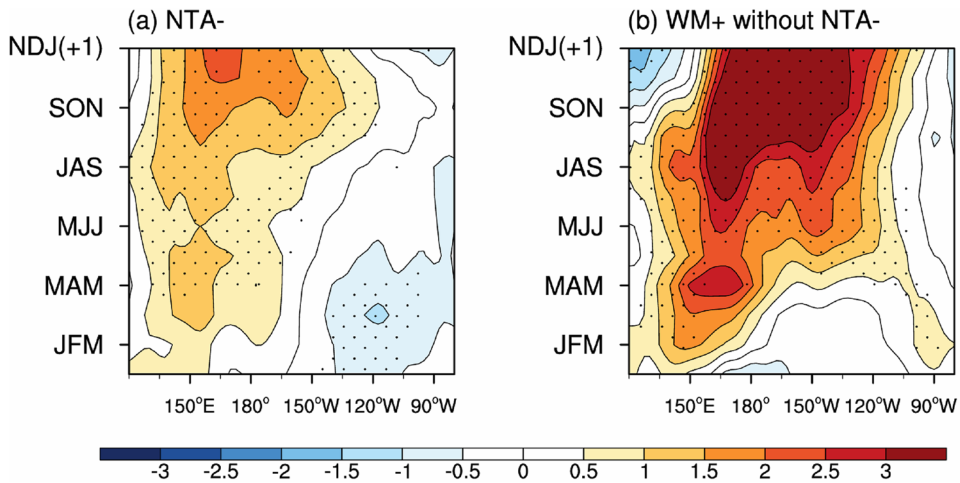

Fig. 13 The longitude-time plot of equatorial Pacific (averaged between 5°S and 5°N) surface wind (vectors, m s^{-1}) anomalies from JFM0 to NDJ (+1) for the strongly negative NTA events (NTA−) (**a**) and positive VM without negative NTA events (VM+without NTA−) (**b**). Stipples indicate anomalies significant at the 95% confidence level. One positive VM event (negative NTA SST events) is defined as a period when the VM index (NTA index) anomaly is greater than (less than) 1 SD

Table 2 Classification of Atlantic and Pacific precursor signals and MAM–SON WWBs activity across six CP El Niño events after the 1990s, Positive (negative) precursor signals denote standardized anomalies exceeding ± 1 standard deviation

CP El Niño event	NAO	NTA	VM	WWBs	Dominant precursor interpretation
1994/95	+	−	No	Suppressed	Atlantic dominated
2002/03	+	−	No	Suppressed	Atlantic dominated
2004/05	No	No	No	No	Pacific internal variability
2009/10	+	−	No	Suppressed	Atlantic dominated
2014/15	+	−	+	Suppressed	Atlantic dominated with VM contribution
2018/19	+	−	No	Suppressed	Atlantic dominated

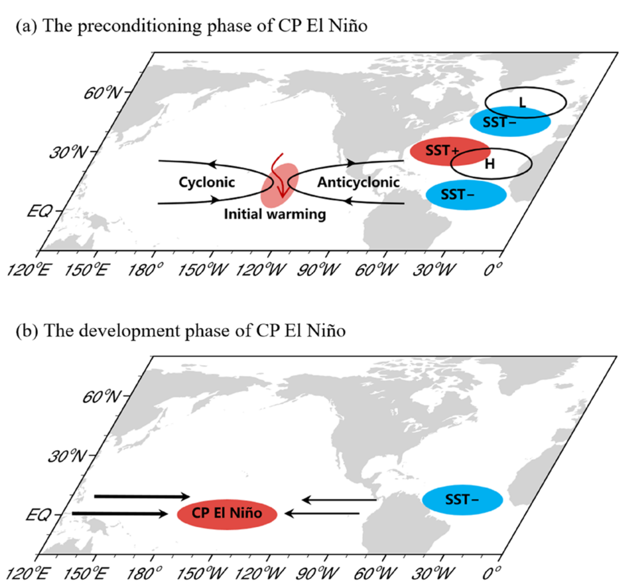

Fig. 14 Schematic diagram of Atlantic air-sea signals through key processes affecting the preconditioning and development phase of CP El Niño events. H and L denote sea level high and low pressure, respectively, and SST + and SST- denote warm SST anomalies and cold SST anomalies, respectively

4 Summary and discussion

In this study, we focused on investigating the impact of Atlantic air-sea signals after the 1990s on CP El Niño events, along with the underlying physical mechanisms responsible for these impacts. Our research findings reveal a marked enhancement in the correlation between CP El Niño variability and the Atlantic air-sea signals after the 1990s, which is characterized by the occurrence of a positive phase of the NAO and a negative NTA mode in the North Atlantic.

It has been discovered that the crucial processes distinguishing CP El Niño events from EP El Niño events lie in the discrepancies in initial warming mechanisms during the preconditioning phase of El Niño events, in addition to the differing timing and locations of the zonal advection feedback and thermocline feedback during the development phase. As summarized by the schematic diagram in Fig. 14, during the initial preconditioning phase, the positive phase of the NAO in the preceding winter drives the emergence of the spring NAT SST pattern, which corresponds to cold SST anomalies in the tropical North Atlantic. The cold NTA SST anomalies induce a pair of cyclones/anticyclones over the tropical Pacific, and the corresponding anomalous southwesterly weaken the intensity of the northeasterly trade winds. This leads to a reduction in sea surface evaporation, and the wind-related LHF triggers the initial warming in the central Pacific through the WES feedback mechanism. During the development phase, the NTA-induced persistent easterly anomalies in the equatorial eastern Pacific impede the functioning of zonal advection feedback in the equatorial eastern Pacific, thereby restricting the eastward spread of warm SST anomalies. Ultimately, such easterly anomalies are conducive to confining anomalous surface warming within the equatorial central Pacific region, which helps shape the characteristic structure of CP El Niño events.

The enhanced influence of Atlantic air–sea signals on CP El Niño after the 1990s is unlikely to result solely from changes within the Atlantic sector. Instead, it may reflect broader multidecadal changes in the tropical climate background state. Previous studies have suggested that the late twentieth-century climate shift was accompanied by strengthened Atlantic–Pacific interactions and changes in the coupled atmosphere–ocean mean state, which can modulate tropical Pacific sensitivity to Atlantic forcing through adjustments in the Walker circulation, trade winds, and air–sea coupling processes (Li et al. 2015; Ding et al. 2023). In addition, Atlantic multidecadal variability has been linked to the increased occurrence of CP El Niño events in recent decades (Yu et al. 2015a, b). Under such conditions, NAO-induced NTA SST anomalies may exert a stronger influence on tropical Pacific atmospheric circulation, thereby facilitating the triggering of CP El Niño events. Nevertheless, the relative contributions of multidecadal climate variability and long-term mean-state changes remain unclear and warrant further investigation.

In addition, although the Indian Ocean Dipole (IOD) is known to influence ENSO variability through atmospheric bridge processes, its peak phase typically occurs in boreal autumn (Saji et al. 1999; Zheng et al. 2021), which is less consistent with the springtime NTA-induced wind anomalies emphasized in this study. In addition, our composite analyses do not reveal a robust or systematic IOD signal preceding CP El Niño events after the 1990s (Fig. 1). This suggests that, while the Indian Ocean may modulate ENSO variability, it is unlikely to be the primary driver of the enhanced CP El Niño occurrence documented here.

In summary, this study provides important insights into the complex interplay among climatic signals, air–sea interactions, and the key processes underlying El Niño diversity. The study's meticulous focus on the heightened incidence of CP El Niño events since the 1990s substantially contributes to our understanding of El Niño dynamics and their implications for climate forecasting and impact assessment.

Acknowledgements This research was funded by the National Key Research and Development Program of China (2022YFF0801701).

Funding The National Key Research and Development Program of China, 2022YFF0801701, Ruiqiang Ding.

Data availability The authors are grateful to all data providers. The datasets utilized in this study are available from http://www.metoffice.gov.uk/hadobs/hadsst3/, https://www.esrl.noaa.gov/psd/data/gridded/data.ncep.reanalysis.html, and https://www.esrl.noaa.gov/psd/data/gridded/data.godas.html.

Declarations

Conflict of interest The authors declare that they have no known competing financial interests or personal relationships that could have appeared to influence the work reported in this paper.

References

Alexander MA, Bladé I, Newman M, Lanzante JR, Lau N-C, Scott JD (2002) The atmospheric bridge: the influence of ENSO Teleconnections on air-sea interaction over the global oceans. J Climate 15(16):2205–2231

Ashok K, Behera SK, Rao SA, Weng H, Yamagata T (2007) El Niño modoki and its possible teleconnection. J Geophys Res Oceans. https://doi.org/10.1029/2006JC003798

Barnston AG, Tippett MK, L'Heureux ML, Li S, DeWitt DG (2012) Skill of real-time seasonal ENSO model predictions during 2002–11: is our capability increasing? Bull Am Meteor Soc 93(5):631–651. https://doi.org/10.1175/BAMS-D-11-00111.1

Behringer DW, Ji M, Leetmaa A (1998) An improved coupled model for ENSO prediction and implications for ocean initialization. Part I: the ocean data assimilation system. Mon Weather Rev 126(4):1013–1021

Bond NA, Overland JE, Spillane M, Stabeno P (2003) Recent shifts in the state of the North Pacific. Geophys Res Lett. https://doi.org/10.1029/2003GL018597

Bretherton CS, Widmann M, Dymnikov VP, Wallace JM, Bladé I (1999) The effective number of spatial degrees of freedom of a time-varying field. J Climate 12(7):1990–2009

Chen D, Lian T, Fu C, Cane MA, Tang Y, Murtugudde R, Song X, Wu Q, Zhou L (2015) Strong influence of westerly wind bursts on El Niño diversity. Nat Geosci 8(5):339–345. https://doi.org/10.1038/ngeo2399

Clarke AJ (2014) El niño physics and el niño predictability. Annu Rev Mar Sci 6:79–99. https://doi.org/10.1146/annurev-marine-010213-135026

Ding R, Li J, Tseng YH, Ruan C (2015a) Influence of the North Pacific Victoria mode on the Pacific ITCZ summer precipitation. J Geophys Res 120(3):964–979. https://doi.org/10.1002/2014JD022364

Ding R, Li J, Tseng YH, Sun C, Guo Y (2015b) The Victoria mode in the North Pacific linking extratropical sea level pressure variations to ENSO. J Geophys Res 120(1):27–45. https://doi.org/10.1002/2014JD022221

Ding R, Nnamchi HC, Yu JY, Li T, Sun C, Li J, Tseng YH, Li X, Xie F, Feng J, Ji K, Li X (2023) North Atlantic oscillation controls multidecadal changes in the North Tropical Atlantic−Pacific connection. Nat Commun 14(1):862. https://doi.org/10.1038/s41467-023-36564-3

Dommenget D, Semenov V, Latif M (2006) Impacts of the tropical Indian and Atlantic Oceans on ENSO. Geophys Res Lett 33(11):11701. https://doi.org/10.1029/2006GL025871

Gill AE (1980) Some simple solutions for heat-induced tropical circulation. Q J R Meteorol Soc 106(449):447–462. https://doi.org/10.1002/qj.49710644905

Ham YG, Kug JS (2015) Role of north tropical Atlantic SST on the ENSO simulated using CMIP3 and CMIP5 models. Clim Dyn 45(11):3103–3117. https://doi.org/10.1007/s00382-015-2527-z

Ham YG, Kug JS, Park JY (2013a) Two distinct roles of Atlantic SSTs in ENSO variability: North Tropical Atlantic SST and Atlantic Niño. Geophys Res Lett 40(15):4012–4017. https://doi.org/10.1002/grl.50729

Ham YG, Kug JS, Park JY, Jin FF (2013b) Sea surface temperature in the north tropical Atlantic as a trigger for El Niño/Southern Oscillation events. Nat Geosci 6(2):112–116. https://doi.org/10.1038/ngeo1686

Hu S, Fedorov A (2018) Cross-equatorial winds control El Niño diversity and change. Nat Clim Change 8(9):798–802. https://doi.org/10.1038/s41558-018-0248-0

Hu X, Yang S, Cai M (2016) Contrasting the eastern Pacific El Niño and the central Pacific El Niño: process-based feedback attribution. Clim Dyn 47(7):2413–2424. https://doi.org/10.1007/s00382-015-2971-9

Huang B, Xue Y, Wang H, Wang W, Kumar A (2012) Mixed layer heat budget of the El Niño in NCEP climate forecast system. Clim Dyn 39(1):365–381. https://doi.org/10.1007/s00382-011-1111-4

Jansen MF, Dommenget D, Keenlyside N (2009) Tropical atmosphere–ocean interactions in a conceptual framework. J Clim 22(3):550–567. https://doi.org/10.1175/2008JCLI2243.1

Jiang L, Li T (2021) Impacts of tropical North Atlantic and equatorial Atlantic SST anomalies on ENSO. J Clim 34(14):5635–5655. https://doi.org/10.1175/JCLI-D-20-0835.1

Kalnay E, Kanamitsu M, Kistler R, Collins W, Deaven D, Gandin L, Iredell M, Saha S, White G, Woollen J, Zhu Y, Chelliah M, Ebisuzaki W, Higgins W, Janowiak J, Mo KC, Ropelewski C, Wang J, Leetmaa A, Joseph D (1996) The NCEP/NCAR 40-year reanalysis project. Bull Am Meteorol Soc 77(3):437–472. https://doi.org/10.1175/1520-0477(1996)077

Kao H-Y, Yu J-Y (2009) Contrasting Eastern-Pacific and Central-Pacific types of ENSO. J Clim 22(3):615–632. https://doi.org/10.1175/2008JCLI2309.1

Kug J-S, Jin F-F, An S-I (2009) Two types of El Niño events: cold tongue El Niño and warm pool El Niño. J Clim 22(6):1499–1515. https://doi.org/10.1175/2008JCLI2624.1

Larkin NK, Harrison DE (2005) On the definition of El Niño and associated seasonal average U.S. weather anomalies. Geophys Res Lett. https://doi.org/10.1029/2005GL022738

Lau N-C (1997) Interactions between global SST anomalies and the midlatitude atmospheric circulation. Bull Am Meteor Soc 78(1):21–34. https://doi.org/10.1175/1520-0477(1997)078

Li X, Xie SP, Gille ST, Yoo C (2015) Atlantic-induced pan-tropical climate change over the past three decades. Nat Clim Change 6(3):275–279. https://doi.org/10.1038/nclimate2840

Li T, Wang B, Wu B, Zhou T, Chang CP, Zhang R (2018) Theories on formation of an anomalous anticyclone in western North Pacific during El Niño: a review. J Meteorol Res 31(6):987–1006. https://doi.org/10.1007/s13351-017-7147-6

McPhaden MJ, Zebiak SE, Glantz MH (2006) ENSO as an integrating concept in earth science. Science 314(5806):1740–1745. https://doi.org/10.1126/science.1132588

Rayner NA, Parker DE, Horton EB, Folland CK, Alexander LV, Rowell DP, Kent EC, Kaplan A (2003) Global analyses of sea surface temperature, sea ice, and night marine air temperature since the late nineteenth century. J Geophys Res Atmos 108(14):4407. https://doi.org/10.1029/2002jd002670

Ren HL, Jin FF (2011) Niño indices for two types of ENSO. Geophys Res Lett. https://doi.org/10.1029/2010GL046031

Rodríguez-Fonseca B, Polo I, García-Serrano J, Losada T, Mohino E, Mechoso CR, Kucharski F (2009) Are Atlantic Niños enhancing Pacific ENSO events in recent decades? Geophys Res Lett 36(20):20705. https://doi.org/10.1029/2009GL040048

Rong XY, Zhang RH, Li T (2010) Impacts of Atlantic sea surface temperature anomalies on Indo-East Asian summer monsoon-ENSO relationship. Chin Sci Bull 55(22):2458–2468. https://doi.org/10.1007/s11434-010-3098-3

Saji NH, Goswami BN, Vinayachandran PN, Yamagata T (1999) A dipole mode in the tropical Indian ocean. Nature 401(6751):360–363. https://doi.org/10.1038/43854

Tian Q, Yu J-Y, Nnamchi HC, Li T, Li J, Li X, Ding R (2025) Unraveling the mystery of recent shortened response time of ENSO to Atlantic forcing. Nat Commun 16(1):5884. https://doi.org/10.1038/s41467-025-61130-4

Wang L, Yu JY, Paek H (2017) Enhanced biennial variability in the Pacific due to Atlantic capacitor effect. Nat Commun 8(1):14887. https://doi.org/10.1038/ncomms14887

Xie SP, Tanimoto Y (1998) A pan-Atlantic decadal climate oscillation. Geophys Res Lett 25(12):2185–2188. https://doi.org/10.1029/98GL01525

Xie R, Jin F-F (2018) Two leading ENSO modes and El Niño types in the Zebiak-Cane model. J Clim 31(5):1943–1962. https://doi.org/10.1175/JCLI-D-17-0469.1

Xu K, Zhu CW, He JH (2012) Linkage between the dominant modes in Pacific subsurface ocean temperature and the two type ENSO events. Chin Sci Bull 57(26):3491–3496. https://doi.org/10.1007/s11434-012-5173-4

Yeh SW, Kug JS, Dewitte B, Kwon MH, Kirtman BP, Jin FF (2009) El Niño in a changing climate. Nature 461(7263):511–514. https://doi.org/10.1038/nature08316

Yeh SW, Kirtman BP, Kug JS, Park W, Latif M (2011) Natural variability of the central Pacific El Niño event on multi-centennial timescales. Geophys Res Lett. https://doi.org/10.1029/2010GL045886

Yeh S-W, Wang X, Wang C, Dewitte B (2015) On the relationship between the North Pacific climate variability and the Central Pacific El Niño. J Clim 28(2):663–677. https://doi.org/10.1175/JCLI-D-14-00137.1

Yu JY, Kim ST (2013) Identifying the types of major El Niño events since 1870. Int J Climatol 33(8):2105–2112. https://doi.org/10.1002/joc.3575

Yu J, Li T, Tan Z, Zhu Z (2015a) Effects of tropical North Atlantic SST on tropical cyclone genesis in the western North Pacific. Clim Dyn 46(3):865–877. https://doi.org/10.1007/s00382-015-2618-x

Yu J-Y, Kao P, Paek H, Hsu H-H, Hung C, Lu M-M, An S-I (2015b) Linking emergence of the Central Pacific El Niño to the Atlantic Multidecadal Oscillation. J Clim 28(2):651–662. https://doi.org/10.1175/JCLI-D-14-00347.1

Zheng X-T, Lu J, Hui C (2021) Response of seasonal phase locking of Indian ocean dipole to global warming. Clim Dyn 57(9):2737–2751. https://doi.org/10.1007/s00382-021-05834-5

Zhong Q, Chan JCL, Duan W et al (2026) Landfalling tropical cyclones accelerate due to land–sea thermal and roughness contrasts. Nat Geosci 19:159–164. https://doi.org/10.1038/s41561-025-01891-1